Progress In Electromagnetics Research, Vol. 134, 359–378, 2013

SYSTEMATIC ANALYSIS OF CONDUCTED ELECTROMAGNETIC INTERFERENCES FOR THE ELECTRIC DRIVE SYSTEM IN ELECTRIC VEHICLES

Yanjie Guo, Lifang Wang*, and Chenglin Liao

Key Laboratory of Power Electronics and Electric Drive, Institute of Electrical Engineering, Chinese Academy of Sciences, No. 6 Beiertiao, Zhongguancun, Beijing, China

Abstract—There are serious electromagnetic compatibility (EMC) problems in electric vehicles. In order to explain and solve them, a systematic method to analyze conducted interferences of the electric drive system is shown in this paper. This method represents the effects of the power battery which is the most different part between electric drive systems used in electric vehicles and other cases. Also, equivalent models are established from power electronics devices to the entire system by considering both the working mechanism and stray parameters. Firstly, insulated gate bipolar transistor (IGBT) and inverter are studied as the main interference source. A new expression is put forward to estimate the frequency domain features of the inverter disturbances. Then, power battery and electric motor are discussed as the main propagation paths. Their high frequency circuit models are given with parameters obtained from tests and measurements. Finally, the system model is established. The system interferences are analyzed to get their generation causes, influence factors and frequency domain characteristics. Comparisons between simulations and experiments verify the correctness of the models and the method.

1. INTRODUCTION

In recent years, researchers have been focusing on the efficiency and reliability of electric vehicle power systems [1]. One of the aspects, the electromagnetic compatibility (EMC) problems of electric vehicles, attracts more attention. There are serious electromagnetic interferences in electric vehicles because some high power equipment

Received 28 September 2012, Accepted 21 November 2012, Scheduled 3 December 2012
* Corresponding author: Lifang Wang (wlf@mail.iee.ac.cn).

works at a high frequency and does on-off operations on high voltages and large currents. Also, large currents rise during short period when starting. These will bring interferences hardly affecting the safety, stability of the vehicles and the heath of the passengers.

Interferences in electric vehicles can be divided into two parts: radiation emission and conducted emission. The former can be analyzed through numerical algorithms of electromagnetic fields, such as finite difference time domain (FDTD) method [2, 3], finite element method (FEM) [4–6] and so on. The latter is what we focus on in this paper. Some methods have been used to reduce the conducted interferences [7], for example, grounding design and the layout design for printed circuit board (PCB). But these methods do not relate to the mechanism of the electric drive system. So they do little help to solve the problem fundamentally. There are some literatures, which study conducted interferences in the electric drive system used in other cases [8]. The research of conducted interference in electric vehicles can obtain the three phase inverter model and common mode (CM) current analysis [9] from these literatures.

In order to investigate EMC problems in electric vehicles, interference sources and propagation paths should be determined. In the electric drive system shown in Fig. 1, considering the steady-state operations of the electric vehicles, the energy flows from the battery to the motor in the driving mode, and the power converter works as an inverter. Besides, energy generated from the motor supplies the battery in the regeneration mode, and the power converter acts as a rectifier. In this system, the main interference source is the power converter which consists of power electronics devices. The conducted interferences caused by power converter flow through battery, motor, cables, coupling capacitances and chassis.

There are literatures investigated conducted interferences of the electric drive system in electric vehicles. Some use statistical methods to get the interference characteristics [10]. However, this

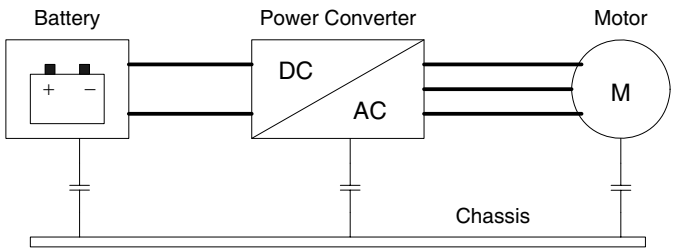

Figure 1. Electric drive system in electric vehicles.

kind of method lacks a theory base and will do harm to the understanding of the interference mechanism. Some study the interference characteristics of electric drive system by using the EMC model of the power converter and the motor [11, 12]. But they ignore stray parameters of power electric devices and power converters, which will lead to inaccurate results, especially in the high frequency range where couplings and resonances caused by stray parameters are dominant. Another research gives the high frequency model of equipments in electric vehicles considering the stray parameters [13]. Nevertheless, it does not discuss the system interference characteristics. Also, an electric drive system model which contains stray parameters of power converters is shown [14, 15]. But it does not express the effects of the battery.

Based on the research above, only the driving mode of steady-state operations is considered. A systematic method to analyze the conducted interferences of the electric drive system in electric vehicles is shown in this paper. This method considers the power battery which has been neglected by the previous research. As an important part, its impedance features have great effects on the disturbances in the electric drive system. Furthermore, this method provides a way to represent the interference characteristics from single device to the high voltage equipments, and then to the entire system. These systematic analyses can make the causes and propagations of the disturbances clearly and easy to develop the suppression programs. So in this paper, the interference characteristics of the main interference source-inverter and insulated gate bipolar transistors (IGBT), which is the basic device of inverter are studied as the interference sources. Then, power battery and electric motor are modeled and analyzed as the interference propagation paths. Finally, the system model is established and the differential mode (DM) and CM interference characteristics are obtained from the simulations and experiments.

2. INTERFERENCE SOURCE EMC MODELS

Essentially, the disturbances of the electric drive system in electric vehicles are generated from the switching processes of power electronics devices. Also, the topology and control strategy of the inverter affect the interference characteristics significantly. So firstly, power electronics devices are discussed. And then, interference source characteristics of the inverter are shown.

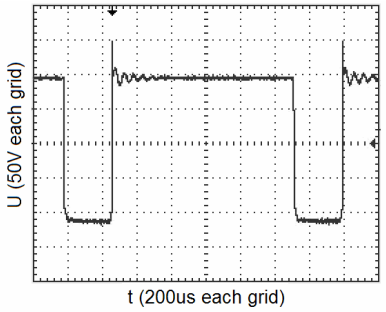

Figure 2. An experimental on-off waveform of IGBT.

Table 1. The frequency ranges of the interference harmonics of IGBT.

	Part. 1)	Part. 2)	Part. 3)
Frequency Range	The switching frequency of IGBT and its multiples	Frequencies much higher than the switching frequency	Frequencies at which the resonances of the stray parameters happen

2.1. Power Electronics Devices

IGBTs are widely used in the electric drive system in electric vehicles. The typical method to analyze their disturbances is to consider the turn-on and turn-off processes [14]. However, the details of on-off processes may not affect the interference characteristics of the equipments and the system much. As shown in Fig. 2, the switching process of IGBT contains three parts: the rectangular pulses, the rising and dropping edges and the over-voltage oscillations which are attributed to stray inductances and capacitances. Hence the corresponding disturbances of IGBT also come from the following three aspects. Also, the frequency ranges of these three parts are given in Table 1.

1) Harmonics at the switching frequency of IGBT and its multiples;
2) High frequency harmonics of the steep rising and dropping edges;
3) Disturbances caused by the stray parameters.

So based on the experimental results, we represent a simple analysis method: discuss the switching process as the interference source firstly, and then consider stray parameters to estimate the influence to the equipments connected with IGBT.

Firstly, rectangular pulses, rising and dropping edges can be described as trapezoidal waves. The spectrum of disturbances generated by these two parts will be given by Eq. (1) through the frequency domain expression of trapezoidal waves.

$$F(k) = \frac{4A_{\max}}{\pi} \frac{T}{2\pi d} \frac{1}{k^2} \left| \sin\left(k \frac{2\pi d}{T}\right) \right| \tag{1}$$

where, $A_{\max}$ is the magnitude, T the period, d the rising and dropping time, and k the order of the harmonics based on the switching frequency.

Then, we can use the spectrum as an interference source to estimate the effects of the stray parameters. Stray parameters of IGBT are shown in Fig. 3, where, U_n is the equivalent interference source of the switching processes, R the resistance of the IGBT, R_g the gate drive resistance, L_g the inductance of the gate connecting wire, L_c and L_e the inductances of connecting wires of the collector and emitter, C_{cg} the stray capacitance between collector and gate, C_{ge} the stray capacitance between gate and emitter, R_{ce} and C_{ce} the stray resistance and capacitance between collector and emitter, R_h and C_h the coupling resistance and capacitance of the heat sink, and C_{GND} the coupling capacitances between connecting cables and the ground.

Some stray parameters of IGBT, such as C_{cg}, C_{ge}, C_{ce}, can be calculated from the parameters in the product data sheet. Other parameters, including inductances of connecting wires and coupling capacities, can be measured directly. So the values of parameters in Fig. 3 are given in Table 2.

Finally, the influences of IGBT are analyzed. Fig. 3 infers that the disturbances of IGBT can disturb equipments in the high voltage

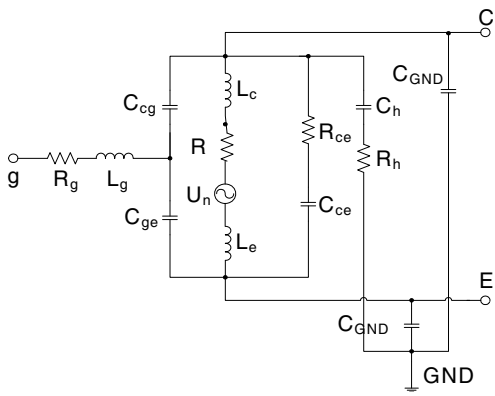

Figure 3. Stray parameters of IGBT.

Table 2. Parameter values in the IGBT equivalent circuit.

C_{cg}	C_{ge}	C_{ce}	R
0.75 µF	10.45 µF	0.5 µF	5.3 mΩ
R_{ce}	L_c	L_e	$C_h,\ C_{GND}$
0.35 mΩ	10 nH	10 nH	1–100 nF

side connected with terminal C, E and devices in the low voltage side with terminal g. Also, CM currents will be generated and flow through coupling capacitances. So transmission gains which express effects of stray parameters can be written by Eq. (2), Eq. (3) and Eq. (4). Where, U_{n1} is the disturbance voltage between C and E; U_{n2} is the disturbance voltage between g and the ground; I_{c1} is the CM currents through the heat sink.

$$\frac{U_{n1}(j\omega)}{U_n(j\omega)} = \frac{\left(R_{ce} + \frac{1}{j\omega \cdot C_{ce}}\right) // \left(\frac{1}{j\omega \cdot C_{cg}} + \frac{1}{j\omega \cdot C_{ge}}\right)}{\left(R_{ce} + \frac{1}{j\omega \cdot C_{ce}}\right) // \left(\frac{1}{j\omega \cdot C_{cg}} + \frac{1}{j\omega \cdot C_{ge}}\right) + R + j\omega \cdot (L_s + L_e)} \tag{2}$$

$$\frac{U_{n2}(j\omega)}{U_n(j\omega)} = \frac{\left(R_{ce} + \frac{1}{j\omega \cdot C_{ce}}\right) // \left(\frac{1}{j\omega \cdot C_{cg}} + \frac{1}{j\omega \cdot C_{ge}}\right)}{\left(R_{ce} + \frac{1}{j\omega \cdot C_{ce}}\right) // \left(\frac{1}{j\omega \cdot C_{cg}} + \frac{1}{j\omega \cdot C_{ge}}\right) + R + j\omega \cdot (L_s + L_e)} * \frac{C_{cg}}{C_{cg} + C_{ge}} \tag{3}$$

$$\frac{I_{c1}(j\omega)}{U_n(j\omega)} = \frac{\left(R_{ce} + \frac{1}{j\omega \cdot C_{ce}}\right) // \left(\frac{1}{j\omega \cdot C_{cg}} + \frac{1}{j\omega \cdot C_{ge}}\right)}{\left(R_{ce} + \frac{1}{j\omega \cdot C_{ce}}\right) // \left(\frac{1}{j\omega \cdot C_{cg}} + \frac{1}{j\omega \cdot C_{ge}}\right) + R + j\omega \cdot (L_s + L_e)} * \frac{1}{R_h + \frac{1}{j\omega \cdot C_h}} \tag{4}$$

Considering the parameter values in Table 1, the above equations suggest that CM currents are related to the coupling parameters between IGBT and the heat sink. The coupling capacitances are small, so the CM currents do not have large values. Also, there are only a few interferences flowing to the low voltage side since the isolated devices exist in the gate drive circuits. So the disturbances generated by IGBT mainly propagate to the high voltage side. In addition, because inductances and capacitances increase with frequency, stray parameters make more effects in the high frequency range.

2.2. Power Converter

Pulse width modulation (PWM) inverter is the main interference source when electric vehicles work in the driving mode. Interferences can be divided into DM and CM interferences both decided by topology of the inverter, IGBT switching processes and PWM control method. Also, stay parameters of the inverter affect the disturbances, especially in the high frequency range. IGBT switching processes controlled by PWM method are the essential reasons causing interferences of the inverter. So we discuss one phase of the inverter firstly. Then, DM and CM interferences are analyzed to get their generation reasons and characteristics. Finally, stray parameters are shown to express their influence.

Firstly, one phase of the inverter is considered. The spectrum of one phase output PWM voltage can be gotten through Fourier transform [16]. However, this method needs lots of calculations and has troubles in actual using. We put forward an approximate estimation for the spectrum of one phase PWM pulses. According to the real inverter in the electric vehicle used for our experiments, we can set the parameters as follows: DC voltage 144 V, basic frequency 50 Hz, carrier frequency 10 kHz, modulation ratio 0.8, rising and dropping time 0.1 µs. So the estimation expression is given by Eq. (5). Comparison between estimated spectrum and spectrum calculated by fast Fourier transform (FFT) is shown in Fig. 4.

$$Spec_{PWM} = \begin{cases} 144 * \frac{2200}{f-400} * \left|\sin c(10^{-6} * (f + 5000))\right| \\ \qquad\qquad\qquad\qquad f \leq 100\,\text{kHz} \\ 144 * 0.5 * \left|\sin c(10^{-4} * (f + 5000))\right. \\ \left. * \sin c(10^{-6} * (f + 5000))\right| \qquad f > 100\,\text{kHz} \end{cases} \tag{5}$$

From Fig. 4, we can see that the estimated spectrum is almost the same as the calculated one and has more deviations in the frequency range higher than 1 MHz. However, the values of spectrum below 1 MHz are about or smaller than 1% of the ones in other frequency ranges. So these deviations will not affect the whole estimation very much. Considering its simple expressions, it would be more effective for the interference analysis.

Then, the DM (u_{ab}, u_{ac} and u_{bc}) and CM (u_{com}) disturbance voltages are defined by Eq. (6) through one phase output PWM voltage u_a, u_b and u_c.

$$\begin{aligned} u_{ab} &= u_a - u_b \\ u_{ac} &= u_a - u_c \\ u_{bc} &= u_b - u_c \\ u_{com} &= u_a + u_b + u_c \end{aligned} \tag{6}$$

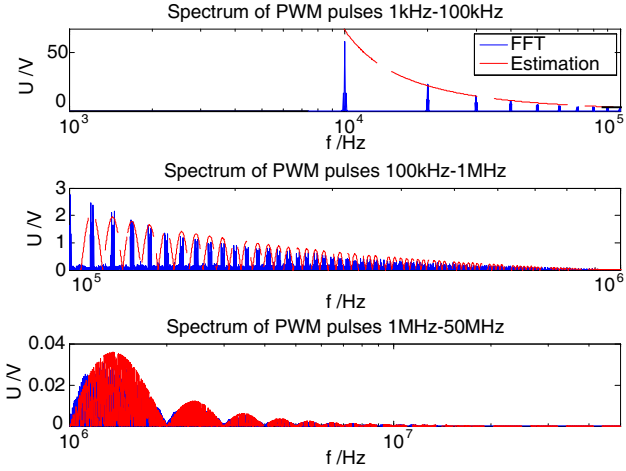

Figure 4. Comparisons between the estimated and calculated spectrums.

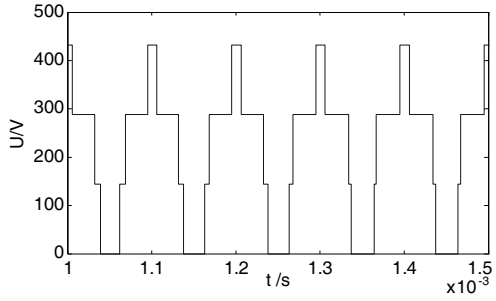

Figure 5. PWM inverter CM disturbance voltage.

The DM interference is caused by different phases of three phase PWM output voltages. It is a kind of functional signal and affects normal operations of the inverter. Unlike DM interference, CM interference generated from the superposition of three phase PWM pulses is not zero. Fig. 5 shows the CM voltage waveform obtained from the same inverter used in the discussions of one phase above, which suggests that the CM interference varies with the carrier frequency, and its peak value is three times of the battery DC voltage. So it will bring serious interferences in the electric vehicles.

Finally, the effects of the stray parameters are considered. A three-phase voltage inverter used for electric vehicle is shown in Fig. 6, where

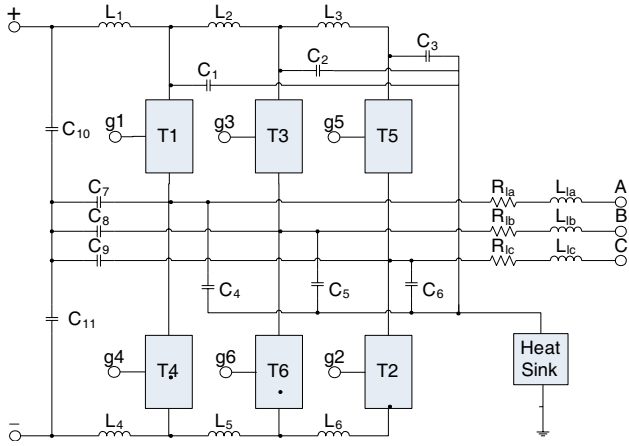

Figure 6. Three-phase inverter model with stray parameters.

the following stray parameters are included.

1) Couplings between DC high voltage side of the inverter and the ground through the heat sink ($C_1 - C_3$) [14];
2) Couplings between three-phase AC output and the ground through the heat sink ($C_4 - C_6$) [14];
3) Resistances and inductances of three-phase AC output cables (R_{la}, L_{la}, R_{lb}, L_{lb}, R_{lc}, and L_{lc});
4) Inductances of DC cables and wires connecting IGBT ($L_1 - L_6$);
5) Couplings between DC side and AC side ($C_7 - C_{11}$) [15].

Summing up the influences of IGBT switching processes, PWM control method, inverter topology and stray parameters, the time and frequency domain characteristics of the inverter are shown as the interference source of the electric drive system in electric vehicles. They will be used for system modeling and interference analysis.

3. PROPAGATION PATH EMC MODELS

The main equipments which disturbances flow through are the power battery and the electric motor. As interference propagation paths, their impedances, especially high frequency impedances, are very important to interference characteristic analysis. So their propagation path models are established based on the impedance characteristics and measured parameters.

3.1. Power Battery

Power battery is one of the principal propagation paths for conducted interferences, but previous research did not include it in the interference analysis of the electric drive system [14, 15]. Some models are established based on the electrochemical features of the power battery [17, 18]. However, these models can not express the high frequency characteristics, which are most important for interference analysis. For some high frequency models [19], they do not consider the energy storage state, which can be described as battery state of charge (SOC). So a new model is represented considering both the high frequency characteristics and the effects of SOC.

The high frequency circuit model of power battery can be expressed as Fig. 7, where L_+, L_- are the inductances of the connecting wires, and R_{g+}, C_{g+}, R_{g-}, C_{g-} are the couplings between the battery and the ground. R_o is the ohm resistance, R_p the polarization resistance, and C_p the polarization capacitance. These battery parameters are all the functions of SOC of the power battery.

According to Fig. 7, the impedance characteristics of interference propagation paths can be studied. The propagation paths are divided into DM and CM interference propagation paths. Their impedance expressions are given by Eq. (7).

$$\begin{aligned} R_{dm}(j\omega) =& (j\omega L_+ + j\omega L_-) + R_o + R_p // \frac{1}{j\omega C_p} \\ R_{com}(j\omega) =& \left(j\omega L_+ + R_{g+} + \frac{1}{j\omega C_{g+}}\right) // \left(j\omega L_- + R_{g-} + \frac{1}{j\omega C_{g-}}\right) \\ & // \left(j\omega L_+ + R_o + R_p // \frac{1}{j\omega C_p} + R_{g-} + \frac{1}{j\omega C_{g-}}\right) \end{aligned} \quad (7)$$

In order to get parameters in the model, power battery used

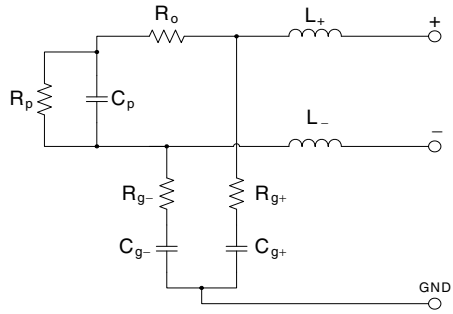

Figure 7. The high frequency circuit model of the power battery.

Table 3. Battery HPPC test results.

SOC	U_{oc} (V)	R_o (Ω)	R_p (Ω)	C_p (F)
0.1	145.35	0.175	0.253	15.81
0.2	148.99	0.148	0.265	15.06
0.3	151.55	0.126	0.267	14.94
0.4	152.98	0.116	0.274	14.55
0.5	153.76	0.112	0.281	14.20
0.6	154.41	0.110	0.286	13.94
0.7	155.27	0.109	0.292	13.66
0.8	156.76	0.112	0.295	13.53
0.9	161.21	0.128	0.288	13.84

in electric vehicles is tested according to the hybrid pulse power characterization (HPPC) test [20], and the results are shown in Table 3.

The parameter identification results suggest: R_o, R_p and C_p do not change too much when SOC varies. So for approximate estimation, the parameters can be given as follows: $R_o = 0.15\,\Omega$, $R_p = 0.28\,\Omega$, $C_p = 15\,\text{F}$. And the battery voltage will not be considered through analysis of interference propagation paths. The inductances of connecting wires and coupling capacities in Fig. 7 are measured and approximately given as follows: $L_+ = L_- = 120\,\text{nH}$, $R_{g+} = R_{g-} = 0.01\,\text{m}\Omega$, $C_{g+} = C_{g-} = 12\,\text{nF}$. So the frequency responses of DM and CM interference voltage-current transfer functions are shown in Fig. 8.

Figure 8(a) suggests that the power battery represents a small resistance to the interferences in the low frequency range. With the frequency increases, the inductances of the connecting wires become dominant and the impedance changes to be inductive gradually. So the battery has suppression on the DM interference in the high frequency range. Its low frequency impedance features are related to the ohm resistance and the polarization resistance, which are both affected by SOC. But the inductances of the connecting wires are dominant in the high frequency range. Fig. 8(b) infers that there is a significant resonance in the CM interference propagation path. It is in the frequency of about 4 MHz, which is the resonance frequency of the inductance of the connecting wires and the coupling capacitance. So these parameters are more decisive in the CM interference propagation path. Taking into account that the interference source contains harmonics in the multiple of 10 kHz, and the small impedance in the resonance frequency, there will be a considerable amount of CM currents flowing through the battery.

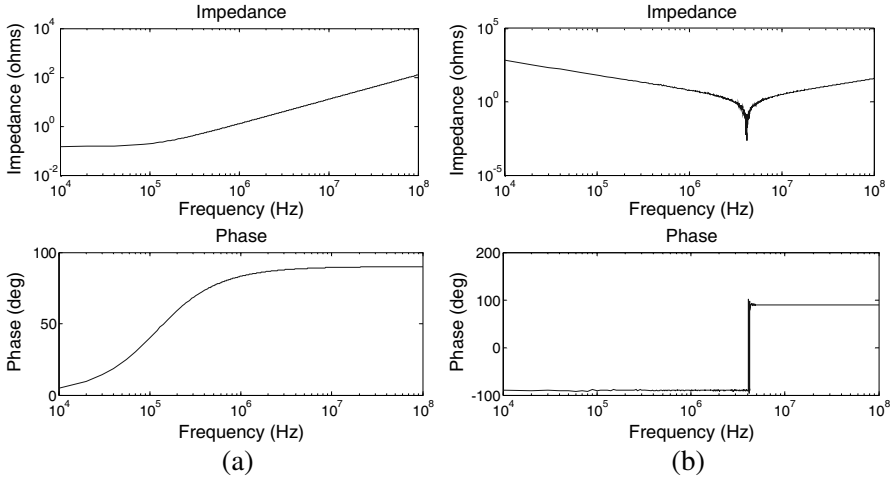

Figure 8. Frequency responses of the battery interference transfer functions. (a) DM interference propagation path. (b) CM interference propagation path.

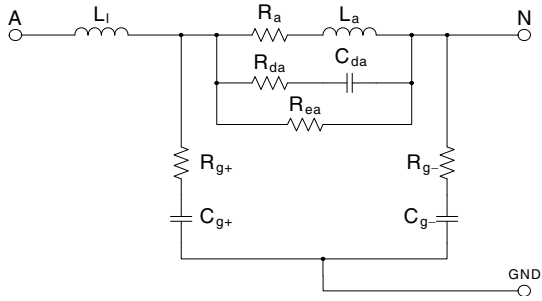

Figure 9. The high frequency circuit model of the electric motor.

3.2. Electric Motor

Electric motor is another main propagation path for conducted interferences in the electric drive system. Based on the electric motor models in reference [21, 22], a model which can simply describe the DM and CM impedances is established and one phase of the electric motor is shown in Fig. 9, where L_l is the inductance of connecting cables; R_a and L_a are resistance and inductance of the winding; R_{da} and C_{da} are couplings between two windings; R_{ea} is used to express the effect of eddy currents. Also, electromagnetic behavior analysis of electric motor can be inferred for establishing the electric motor model [23].

According to the high frequency circuit model in Fig. 9, the impedance characteristics of interference propagation paths can be analyzed. Like the battery, propagation paths of the motor are also divided into DM part and CM part and their impedance expressions are given by Eq. (8).

$$\begin{aligned} R_{dm}(j\omega) =& j\omega L_l + (R_a + j\omega L_a) // \left(R_{da} + \frac{1}{j\omega C_{da}}\right) // R_{ea} \\ R_{com}(j\omega) =& j\omega L_l + \left(R_{g+} + \frac{1}{j\omega C_{g+}}\right) // \left[\left(R_{g-} + \frac{1}{j\omega C_{g-}}\right)\right. \\ & \left. + (R_a + j\omega L_a) // \left(R_{da} + \frac{1}{j\omega C_{da}}\right) // R_{ea}\right] \end{aligned} \tag{8}$$

The parameters in Fig. 9 can be obtained from several tests and measurements. Firstly, the winding resistance R_a is identified by the locked rotor experiments, and the results are shown in Table 4. It infers that average winding resistance is $0.032\,\Omega$. The other parameters can also be measured or calculated [21] and approximately given in Table 5. So the frequency responses of DM and CM interference voltage-current transfer functions are shown in Fig. 10.

Figure 8(a) suggests that the motor has more complex DM impedances than the battery. In the low frequency range, the winding inductance is decisive so the DM impedance is inductive.

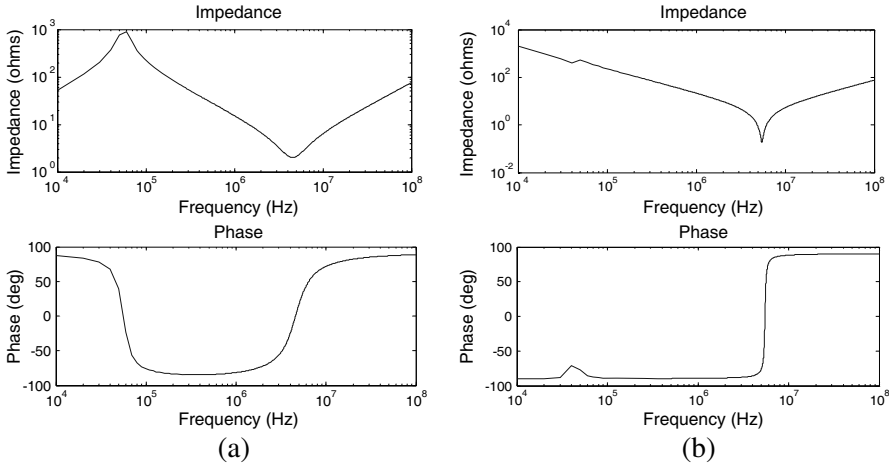

Figure 10. Frequency responses of the motor interference transfer functions. (a) DM interference propagation path. (b) CM interference propagation path.

Table 4. Results of the locked rotor experiments.

U (V)	I_a (A)	R_a (Ω)
1.35	46.0	0.02935
1.06	30.2	0.03510
1.05	30.5	0.03443
1.47	48.2	0.03050
1.17	50.4	0.02917

Table 5. Parameter values in the motor equivalent circuit.

L_a	L_l	R_{da}	R_{ea}
800 µH	120 nH	2 Ω	1 kΩ
C_{ea}	R_{g+}, R_{g-}	C_{g+}, C_{g-}	
10 nF	0.01 mΩ	12 nF	

Then the coupling capacitance between windings begins to work, and the impedance changes to be capacitive gradually. Finally, the inductances of the connecting wires become dominant with the frequency increases as the same as the power battery. So the electric motor restrains interferences in low and high frequency ranges, but increases interferences in the middle frequency range. In the CM path, it is like the power battery which has a significant resonance as shown in Fig. 8(b). This similarity can be explained by that the battery and the motor have the similar parameters of connecting wire inductances and coupling capacities, which are dominant in the CM interference propagation paths. Also, there will be a considerable amount of CM currents flowing through the motor.

4. SYSTEM INTERFERENCE ANALYSIS

Since the models of main equipments of the electric drive in electric vehicles are given above, we can sum them up to analyze the interferences systematically. The system model is established based on a real electric vehicle. The electric drive system mainly contains a nickel-metal hydride (Ni-MH) battery with 144 V normal rated voltage, a three phase voltage inverter with 10 kHz carrier frequency, a permanent magnet synchronous motor (PMSM) with 13 kW normal rated power and several connecting cables. These equipments used in the electric vehicle are the same as the ones used for the interference source and propagation path analysis in Sections 2 and 3.

To analyze problems in detail, we select two typical signals to verify the system model and show the interference characteristics. They are the DM disturbance voltage of the PWM inverter output and the CM disturbance currents of the DC bus. The system model is simulated through MTALAB and the results are shown in Fig. 11. The compared experimental waveforms and spectrums are given in Fig. 12.

The simulated and experimental results of DM disturbance voltage and CM disturbance currents are almost the same as shown in Fig. 11 and Fig. 12. So the established system model can describe the interference characteristics of the actual electric drive system. The results also infer that the main interference frequencies of the DM

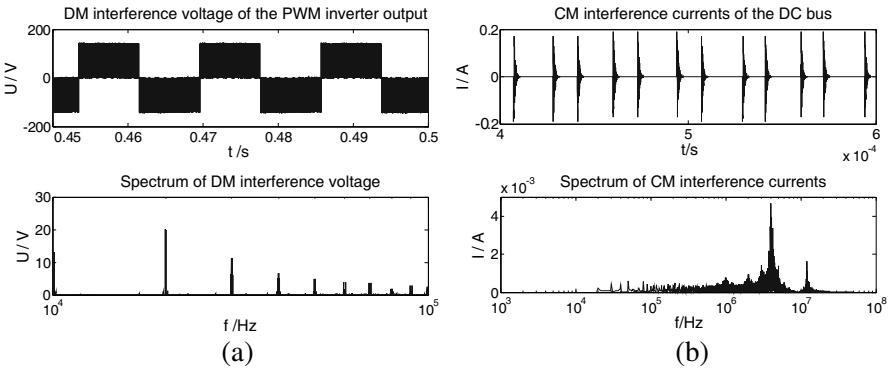

Figure 11. Simulation results. (a) Waveform and spectrum of DM disturbance voltage of the PWM inverter output. (b) Waveform and spectrum of CM disturbance currents of the DC bus.

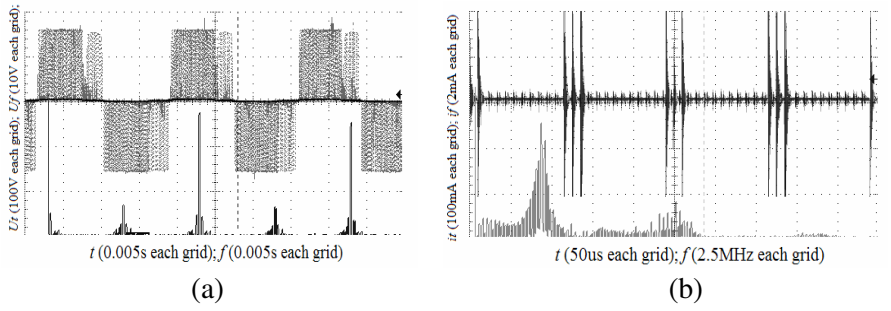

Figure 12. Experimental results. (a) Waveform and spectrum of DM disturbance voltage of the PWM inverter output. (b) Waveform and spectrum of CM disturbance currents of the DC bus.

disturbance voltage are the multiples of the carrier frequency of the inverter. Hence, the DM interferences are a kind of fundamental waveforms related to the normal working of the PWM inverter. So they can only be reduced but not cancelled. Unlike the DM interferences, CM interference currents are decided more by the stray coupling parameters. They can bring severe problems owing to their high frequency, which makes them propagate through coupling capacities and radiation emissions easily. So we will discuss more details of the system CM interference characteristics as follows.

The comparison between CM disturbance voltage and currents is shown in Fig. 13(a). It suggests that the oscillations of CM currents occur when the CM voltage changes, because there are many high

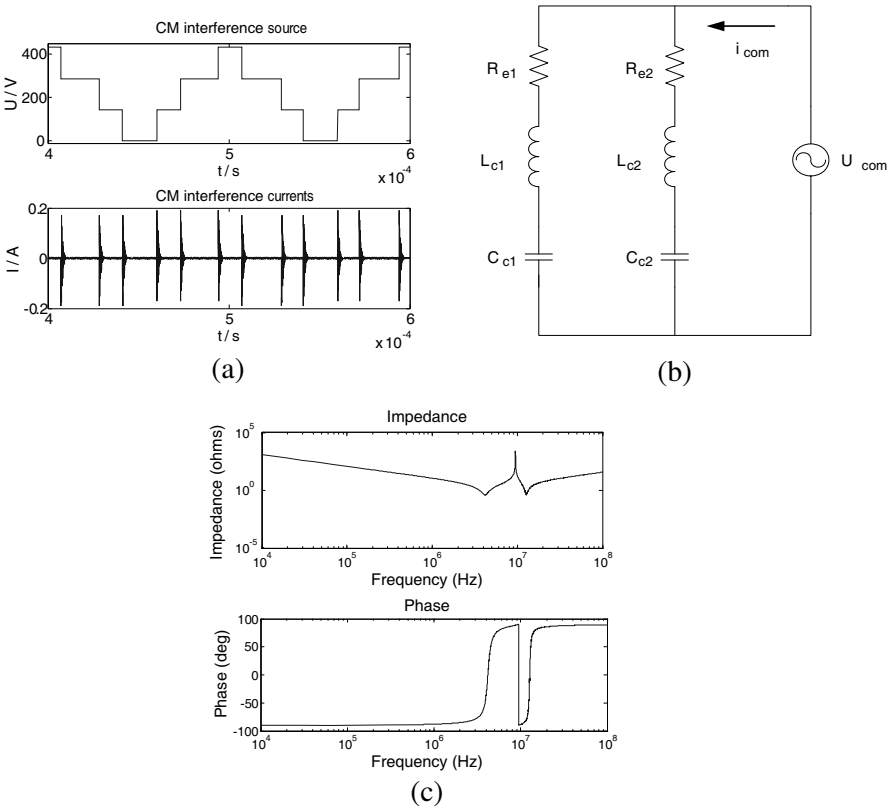

Figure 13. (a) Comparison between CM interference source and CM currents. (b) System CM equivalent circuit. (c) System CM interference propagation path frequency response.

frequency harmonics in the rising and dropping edges when the CM voltage changes. Only these high frequency harmonics can propagate through the coupling capacities. The appearance of CM currents explains that the effects of propagation path impedances are more decisive rather than the interference source.

Figures 11(b) and 12(b) infer that there are two main resonance frequencies in the CM propagation paths of the electric drive system: about 4 MHz and 12.5 MHz. Considering the experimental spectrum of the CM interferences in reference [14], it also contains two main interference frequencies about several megahertz. Hence, it can be proved that some common features of the CM interference are obtained in this paper. These main interference frequencies can be thought as resonances of connecting wire inductances and coupling capacities. So the system CM equivalent circuit can be depicted as Fig. 13(b), where L_{c1} and C_{c1} are the first group of resonance parameters with 4 MHz; L_{c2} and C_{c2} are the second group of resonance parameters with 12.5 MHz; R_{e1} and R_{e2} are used to express the impacts of eddy currents in chassis and other conductors which CM currents flow through. L_{c1} is 120 nH ,and C_{c1} is 12 nF, both the same as the parameters in the battery and motor equivalent model. They have a resonance frequency of 4 MHz. Coupling capacities have different values with different coupling distances while the connecting wire inductances do not change too much. Hence, C_{c2} reduces to 1.3 nF, and L_{c2} still keeps 120 nH. Based on the parameters, the frequency response of system CM interference voltage-current transfer function is given in Fig. 13(c). It shows that there are significant resonances at the frequency of about 4 MHz and 12.5 MHz. So the equivalent circuit in Fig. 13(b) can approximately describe the CM interference paths of the electric drive system in electric vehicles.

5. CONCLUSION

A systematic analysis of conducted interferences for the electric drive system in electric vehicles is represented in this paper. The models of IGBT, inverter, motor and the entire system are established. A new expression is put forward to estimate the spectrum of the PWM inverter. Furthermore, the power battery which is the most different part between electric drive systems used in electric vehicles and other cases is analyzed to show its impedance features as interference propagation paths. These models define the interference source and propagation paths clearly and have considered both the working mechanism and the influences of stray parameters. Through identifying the parameters of these models, the time domain and

frequency domain characteristics are studied systematically from power electronics devices to the whole electric drive system. The method, models and analyses are verified by both simulations and experiments. The systematic method shown in this paper can be used for predictions of the time domain and frequency domain interference characteristics of the electric drive system in electric vehicles. It can also help interference suppression, EMC designs and to reduce costs in the development of electric vehicles.

ACKNOWLEDGMENT

Authors are gratefully acknowledging the support by Chinese National High-tech R&D (863 program) Project (2011AA11A262).

REFERENCES

1. Mahmoudi, A., N. A. Rahim, and W. P. Hew, "Axial-flux permanent-magnet motor design for electric vehicle direct drive using sizing equation and finite element analysis," *Progress In Electromagnetics Research*, Vol. 122, 467–469, 2012.
2. Lei, J.-Z., C.-H. Liang, W. Ding, and Y. Zhang, "EMC analysis of antennas mounted on electricity large platforms with parallel FDTD methods," *Progress In Electromagnetics Research*, Vol. 84, 205–220, 2008.
3. Ala, G., M. C. Di Piazza, G. Tinè, et al., "Evaluation of radiated EMI in 42-V vehicle electrical systems by FDTD simulation," *IEEE Trans. Vehicular Technology*, Vol. 56, No. 4, 1477–1484, Jul. 2007.
4. Lecointe, J.-P., B. Cassoret, and J.-F. Brudny, "Distinction of toothing and saturation effects on magnetic noise of induction motors," *Progress In Electromagnetics Research*, Vol. 112, 125–137, 2011.
5. Jian, L. and K.-T. Chau, "Design and analysis of a magnetic-geared electronic-continuously variable transmission system using finite element method," *Progress In Electromagnetics Research*, Vol. 107, 47–61, 2010.
6. Touati, S., R. Ibtiouen, O. Touhami, and A. Djerdir, "Experimental investigation and optimization of permanent magnet motor based on coupling boundary element method with permeances network," *Progress In Electromagnetics Research*, Vol. 111, 71–90, 2011.

7. Wu, Q., X. Zhang, L. Wang, et al., "EMC design for HEV drive system," *IEEE International Symposium on Microwave, Antenna, Propagation, and EMC Technologies for Wireless Communications*, 1361–1364, Hangzhou, China, 2007.
8. Revol, B., J. Roudet, J.-L. Schanen, et al., "EMI study of three-phase inverter-fed motor drives," *IEEE Trans. Industry Applications*, Vol. 47, No. 1, 223–231, Jan.–Feb. 2011.
9. Akagi, H. and T. Doumoto, "An approach to eliminating high-frequency shaft voltage and ground leakage current from an inverter-driven motor," *IEEE Trans. Industry Applications*, Vol. 40, No. 4, 1162–1169, Jul.–Aug. 2004.
10. Li, W., S. Yu, B. Zhang, J. He, et al., "A statistical model of noises at input port of inverter and its coupling to low voltage cable on fuel cell bus," *IEEE International Symposium on Electromagnetic Compatibility*, 1–6, Hawaii, USA, 2007.
11. Labrousse, D., B. Revol, and F. Costa, "Common-mode modeling of the association of N-switching cells: Application to an electric-vehicle-drive system," *IEEE Trans. Power Electronics*, Vol. 24, No. 11, 2852–2859, Nov. 2010.
12. Li, W., S. Yu, B. Zhang, J. He, et al., "High frequency conducted disturbance analysis of driving system in fuel cell vehicle," *The 4th Asia-Pacific Conference on Environmental Electromagnetics*, 724–727, Dalian, China, 2006.
13. Guttowski, S., S. Weber, E. Hoene, et al., "EMC issues in cars with electric drives," *IEEE International Symposium on Electromagnetic Compatibility*, 777–782, Istanbul, Turkey, 2003.
14. Lee, Y. H. and A. Nasiri, "Analysis and modeling of conductive EMI noise of power electronics converters in electric and hybrid electric vehicles," *Applied Power Electronics Conference and Exposition*, 1952–1957, Austin, USA, 2008.
15. Chen, S., T. W. Nehl, J. S. Lai, et al., "Towards EMI prediction of a PM motor drive for automotive applications," *Applied Power Electronics Conference and Exposition*, 14–22, Miami, USA, 2003.
16. Mohan, N., T. M. Undeland, and W. P. Robbins, *Power Electronics Converters, Applications and Design*, 3rd Edition, Wiley, 2003.
17. Chen, M. and G. A. Rincon-Mora, "Accurate electrical battery model capable of predicting runtime and I-V performance," *IEEE Trans. Energy Conversion*, Vol. 21, No. 2, 504–511, Jun. 2006.
18. Gao, L., S. Liu, and R. A. Dougal, "Dynamic lithium-ion battery model for system simulation," *IEEE Trans. Components and*

Packaging Technologies, Vol. 25, No. 3, 495–505, Sep. 2002.

19. Hoene, E., S. Guttowski, R. Saikly, et al., "RF-properties of automotive power batteries," *IEEE International Symposium on Electromagnetic Compatibility*, 425–428, Istanbul, Turkey, 2003.
20. Hunt, G., "Freedom car battery test manual for power-assist hybrid electric vehicles," INEEL, Idaho Falls, 2003.
21. Boglietti, A., E. Carpaneto, and P. di Torino, "Induction motor high frequency model," *IEEE Industry Applications Conference, 34th IAS Annual Meeting*, 1551–1558, Phoenix, USA, 1999.
22. Mirafzal, B., G. Skibinski, R. Tallam, et al., "Universal induction motor model with low-to-high frequency response characteristics," *Industry Applications Conference, 41st IAS Annual Meeting*, 423–433, Tampa, USA, 2006.
23. Liang, J., L. Jian, G. Xu, and Z. Shao, "Analysis of electromagnetic behavior in switched reluctance motor for the application of integrated air conditioner on-board charger system," *Progress In Electromagnetics Research*, Vol. 124, 347–364, 2012.